

We are IntechOpen, the world's leading publisher of Open Access books Built by scientists, for scientists

6,900

Open access books available

186,000

International authors and editors

200M

Downloads

Our authors are among the

154

Countries delivered to

TOP 1%

most cited scientists

12.2%

Contributors from top 500 universities



WEB OF SCIENCE™

Selection of our books indexed in the Book Citation Index
in Web of Science™ Core Collection (BKCI)

Interested in publishing with us?
Contact book.department@intechopen.com

Numbers displayed above are based on latest data collected.
For more information visit www.intechopen.com



Study on the Interaction Between Tsunami Bore and Cylindrical Structure with Weir

I. Wijatmiko and K. Murakami
*University of Miyazaki
Japan*

1. Introduction

The destructive power of tsunami creates catastrophic damages in large area. In order to reduce these damages, there is a need to understand the interactions between tsunami wave and structures as the basic knowledge before applying any countermeasure strategies.

Tsunami amplifies its height in shallow water area, and it may transfer into bore when it breaks and generates enormous forces (Yeh, 1991). The impact of tsunami bore to the vertical structures with two-dimensional cross section has been investigated through experiments and numerical simulations (Fukui et al., 1962; Palermo & Nistor, 2008). Those previous studies provide many useful information for the construction of coastal structures. However, the interaction between tsunami bore and structures with three-dimensional cross section have not been understood well, because tsunami flow around such structures becomes quite complex. Structures with three-dimensional section, such as a storage tank and tsunami evacuation building, can be seen as important infrastructures on many coastal areas. Especially, the recent tsunami Japan 2011 had brought serious damages on structures such as oil storages (International Energy Agency, 2011). Meanwhile, those structures are regulated by a building code to be protected by weir to restrain the spread of spilled contents (Dangerous Goods Safety Management [DGSM], 2003). This protective weir may produce quite complex flow around the structures, but the effects of the flow on the structures with weir have not been investigated well.

In the investigation of interactions between tsunami wave and cylindrical structure, a numerical simulation is very powerful tools to obtain much detail quantities such as pressures, velocities and free surface elevations, at any points with higher resolution in time and space. Recently, many numerical simulation techniques have been developed in order to simulate wave motions around three-dimensional structures (Arikawa & Yamano, 2008; Goto et al., 2009; Tomita et al., 2006; Kawasaki et al., 2006). Among those numerical models, the method based on Navier-Stokes equation and Volume of Fluid (VOF; CADMAS-SURF 3D) tends to be used as one of the common numerical technique to simulate three-dimensional interactions between wave and structures (Arikawa & Yamano, 2008).

This study investigates the validity of three dimensional numerical simulation model based on Navier-Stokes equation and VOF method to estimate hydraulic quantities around the structure. Furthermore, this study discusses the characteristics of interaction between bore type tsunami and the cylindrical structure with weir with using above numerical model.

2. Background

2.1 Previous study

An extensive summary on the bore type tsunami propagation is given by Yeh (1991). Here the focus is on the bore type tsunami behaviours and its transition process along the shore. This process is caused by the 'momentum exchange' between the bore and the small wedge-shaped water body. It has been studied that the changes of velocities and the convergence of fluid tend to accumulate turbulence on the front face of the bore when the bore reach the shoreline. In addition, the no-water condition in front of bore cause wave flow to rely on its velocity for the run-up motion, and it causes stronger turbulence on the transition process. The generated turbulence and its accumulation, together with rapidly accelerated mean flow motion, are said to be the cause of destructive tsunami energy on the dry beach surface. Mizutani & Imamura (2001) investigated the destructive tsunami pressure on the breakwaters by using the highly accurate sensor system. They categorized the type of maximum pressure such as: dynamic pressure, sustain pressure, impact standing pressure and overflowing wave pressure. The dynamic pressure occurs when an incident wave hits structures at the first attempt. After this pressure, the sustain pressure is observed due to the succeeding tsunami flow. In addition, the impact standing pressure may occur when the reflected tsunami wave coincide with incoming wave. While the overflowing wave pressure occurs when wave collide on the back of the structure. Another investigation of tsunami risk to structures had been done by Palermo & Nistor (2008). The tsunami-induced loading and its impact on the shoreline structure according to Canadian context were mainly discussed. Several physical experiments had been done for the purpose of understanding Tsunami forces acting on the structure. Several structural shapes, such as square, rectangular, diamond-shape and cylindrical shape, and also debris impact testing were discussed in this study. Through various cases of experiments, the result indicated that through various impoundment heights, the force caused by surge wave does not significantly exceed the drag force. Further, the existence of debris can generate the 'bounce back' effect on the structure, even though the magnitude of this force was smaller than the initial debris impact. This study emphasized the consideration of tsunami-induced loading for the structures.

Haritos, Ngo & Mendis in 2005 gave the brief review on the estimation of tsunami wave force on wall structures by many coastal engineers. Japanese researchers purposed estimations of wave pressure on the building face in the case of 'unbroken' and 'break-up' tsunami conditions (Okada et al., 2004). In the case of 'unbroken' tsunami condition, the hydrostatic distribution reaches up to 3 times of wave height with maximum pressures located at the bottom section of building. Meanwhile, this estimation is superimposed by $2.4 \rho gh$, where ρ is water density; g is gravity and h is wave height at 0.8 of maximum wave height above the ground for the case of 'break-up' tsunami. Meanwhile The U.S. Army Corps gave an assumption that the interaction between surge wave and structure consist of hydrostatic action and hydrodynamic one. In addition, the dynamic action is calculated based on the bore gradient on its face (U.S. Army Corps, 1990, as cited in Haritos, N., et al., 2005).

An extensive description of tsunami load acting on shoreline structure was provided by Yeh, H. (2007). Tsunami load was analysed with considering: 1) hydrostatic force, 2) buoyant force, 3) hydrodynamic force, 4) surge force, 5) debris impact force, and 6) wave breaking force. Among these forces, hydrodynamic force and surge force give significant contribution to the maximum force acting on structures. Further, the Federal Emergency Management Agency's Coastal Construction Manual in 2008 mentions the additional estimation beside those forces, such as uplift force and gravity loads in case of building with elevated floors.

2.2 Theoretical considerations

2.2.1 Hydrodynamic model

The evolution of tsunami wave with time can be expressed by a system of nonlinear partial differential equations. However, these equations are very difficult to solve analytically. Therefore, a numerical method that discretizes a computational domain into grids is sometimes used to obtain tsunami wave field. There are several numerical methods to solve fluid dynamic problems, e.g. the finite difference method (fdm), the finite element method (fem) and the finite volume method (fvm). The finite difference method, which discretizes a computational domain into square cells with fix width (Δx), length (Δy) and height (Δz) in a three dimensional problem, is widely used to solve many hydraulic problems. However, the square grid sometimes loses the resolution of boundary shapes, which can be seen on the structure with complex cross sections. On the other hand, the finite element method allows various grid sizes, and it can be applied to the structure with complex shape.

With the increase of computer capacity, some direct numerical simulation techniques have being developed recently in coastal engineering field to investigate the interaction problems between waves and structures. The basic equations in this direct numerical simulation are the continuity equation and momentum equations witch is called Navier-Stokes equation. This study employs a system of above equations, those are discretizes with the finite difference method to simulate tsunami flow around three-dimensional structure on arbitrary topography.

2.2.2 Governing equations

The governing equations used in this study are the continuity equations expressed in Eq.(1) and momentum ones from Eq.(2) to Eq.(4). The system of these equations is purposed by Sakakiyama & Kajima (1992), where the area porosities $\gamma_x, \gamma_y, \gamma_z$ in x, y and z projections are introduced respectively in order to investigate the interactions between waves and porous structures.

$$\frac{\partial \gamma_x u}{\partial x} + \frac{\partial \gamma_y v}{\partial y} + \frac{\partial \gamma_z w}{\partial z} = \gamma_v S_p \quad (1)$$

$$\begin{aligned} \lambda_v \frac{\partial u}{\partial t} + \frac{\partial \lambda_x u u}{\partial x} + \frac{\partial \lambda_y v u}{\partial y} + \frac{\partial \lambda_z w u}{\partial z} = & -\frac{\gamma_v}{\rho} \frac{\partial p}{\partial x} + \frac{\partial}{\partial x} \left\{ \gamma_x v_e \left(2 \frac{\partial u}{\partial x} \right) \right\} + \frac{\partial}{\partial y} \left\{ \gamma_y v_e \left(\frac{\partial u}{\partial y} + \frac{\partial v}{\partial x} \right) \right\} \\ & + \frac{\partial}{\partial z} \left\{ \gamma_z v_e \left(\frac{\partial u}{\partial z} + \frac{\partial w}{\partial x} \right) \right\} - \gamma_v D_x u - R_x + \gamma_v S_u \end{aligned} \quad (2)$$

$$\lambda_v \frac{\partial v}{\partial t} + \frac{\partial \lambda_x uv}{\partial x} + \frac{\partial \lambda_y vw}{\partial y} + \frac{\partial \lambda_z wv}{\partial z} = -\frac{\gamma_v}{\rho} \frac{\partial p}{\partial y} + \frac{\partial}{\partial x} \left\{ \gamma_x v_e \left(\frac{\partial v}{\partial x} + \frac{\partial u}{\partial y} \right) \right\} + \frac{\partial}{\partial y} \left\{ \gamma_y v_e \left(2 \frac{\partial v}{\partial y} \right) \right\} + \frac{\partial}{\partial z} \left\{ \gamma_z v_e \left(\frac{\partial v}{\partial z} + \frac{\partial w}{\partial y} \right) \right\} - \gamma_v D_y v - R_y + \gamma_v S_v \quad (3)$$

$$\lambda_v \frac{\partial w}{\partial t} + \frac{\partial \lambda_x uw}{\partial x} + \frac{\partial \lambda_y vw}{\partial y} + \frac{\partial \lambda_z ww}{\partial z} = -\frac{\gamma_v}{\rho} \frac{\partial p}{\partial y} + \frac{\partial}{\partial x} \left\{ \gamma_x v_e \left(\frac{\partial w}{\partial x} + \frac{\partial u}{\partial z} \right) \right\} + \frac{\partial}{\partial y} \left\{ \gamma_y v_e \left(\frac{\partial w}{\partial y} + \frac{\partial v}{\partial z} \right) \right\} + \frac{\partial}{\partial z} \left\{ \gamma_z v_e \left(2 \frac{\partial w}{\partial z} \right) \right\} - \gamma_v D_z w - R_z + \gamma_v S_w - \frac{\gamma_v \rho^* g}{\rho} \quad (4)$$

where t is the time, x and y the horizontal coordinates, z the vertical coordinate, u, v, w the velocity components in the direction of x, y and z respectively. ρ means the density of the fluid, ρ^* the relative density of the fluid, p the pressure. v_e means the kinematic viscosity (summation of molecular kinematic viscosity and eddy kinematic viscosity), g the gravity, λ_v is defined from γ_v using following relationships:

$$\lambda_v = \gamma_v + (1 - \gamma_v) C_M \quad (5)$$

where C_M is the inertia coefficient. While the resistance force R_x, R_y and R_z are described in Eq. (6), Eq. (7) and Eq. (8).

$$R_x = \frac{1}{2} \frac{C_D}{\Delta x} (1 - \gamma_x) u \sqrt{u^2 + v^2 + w^2} \quad (6)$$

$$R_y = \frac{1}{2} \frac{C_D}{\Delta y} (1 - \gamma_y) v \sqrt{u^2 + v^2 + w^2} \quad (7)$$

$$R_z = \frac{1}{2} \frac{C_D}{\Delta z} (1 - \gamma_z) w \sqrt{u^2 + v^2 + w^2} \quad (8)$$

where C_D is the drag coefficient; $\Delta x, \Delta y$ are the horizontal mesh sizes and Δz is the vertical mesh sizes in porous media.

2.2.3 Boundary condition and discretization of numerical domain

Volume of Fluid (VOF) method, which was introduced by Hirt & Nichols in 1981, is used in this study to distinguish the air and water zone. A function, F , is introduced in the VOF method to define the fluid region. This function indicate the fractional volume of water which occupies each cell in the computational domain. Youngs (1982) described the algorithm to track the interface between air and water zone. In the first step, the interface is approximated by a linear line in each cell. After that, the interface is detected by solving a advection equation, which relates to the function, F , in order to get the evolution of fractional function in time series. The three-dimensional advection equation for fractional function is described in Eq. (9).

$$\gamma_v \frac{\partial F}{\partial t} + \frac{\partial \gamma_x u F}{\partial x} + \frac{\partial \gamma_y v F}{\partial y} + \frac{\partial \gamma_z w F}{\partial z} = \gamma_v S_F \quad (9)$$

This study generates the bore type tsunami in developed numerical flume. The fluid motion start from a still water condition. The initial pressure is given by hydrostatic pressure, where the water density is 998.2 kg/m^3 and air density is 1.2 kg/m^3 . In this study, slip condition is applied in the interface between fluid and solid boundary.

In order to propagate bore type tsunami, time history of wave surface elevation and fluid velocity are set as the initial flow parameters in the ghost cells which is set at outside of the most upstream cells. These values will be calculated by using the governing equation for the rest of the domain.

Fukui, et.al had investigate the relations between fluid mean velocity and water surface displacement under the propagation of bore type tsunami. Through analytical investigation and a series of hydraulic experiments, they derived the following equation.

$$U = \frac{c\zeta}{H} = \zeta \sqrt{\frac{gH(H+h)}{2H(H+\eta\zeta)}} \quad (10)$$

where U is the mean velocity, g the acceleration of gravity, $H=h+\zeta$ the total depth from the datum (Refer to Fig.1), ζ the temporal bore height. η is the velocity coefficients, which equal to 1.03, and it was taken from the ratio of water level and wave height.

In this study, the water surface profile of bore type tsunami on the most upstream boundary is assumed at first, and the velocity profile on the same boundary is obtained from Eq.(10).

Finite difference method with staggered grid mesh is applied to discretize the governing equations. The velocity components are defined on the each boundary of the cell, while scalar quantities, such as pressure and F-function, are defined at the center of the cell. Finite control volume is applied to satisfy the conservation equation for momentum equation. Both central difference technique and upwind scheme are used to discretize the spatial derivative, while F-function is discretize by using forward difference method. The simplified marker and cell (SMAC) method is used to estimate the time evolution solution for continuity and momentum equations.

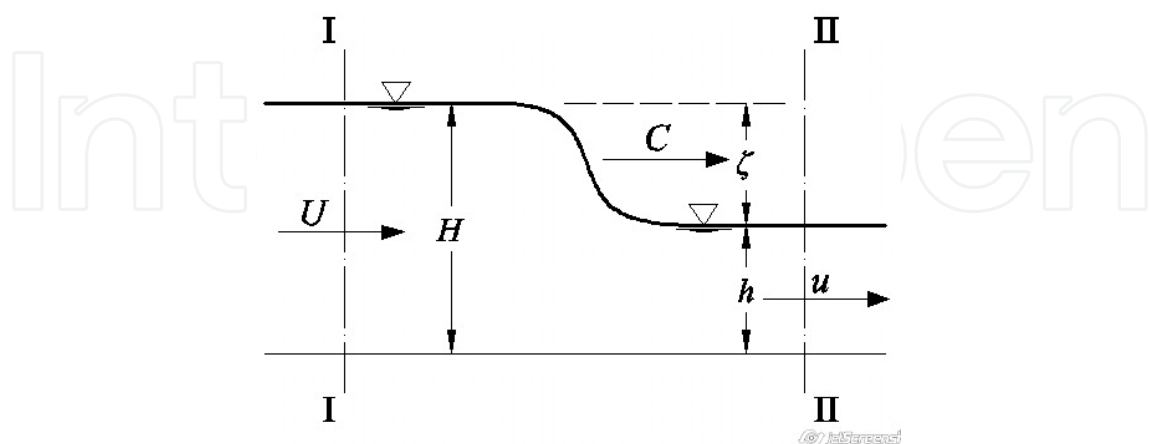


Fig. 1. Bore profile illustration

3. Hydraulic experiments for the verification of numerical simulation

In order to investigate the validity of numerical simulation, some numerical results are compared with experimental ones. This study examined the validity of numerical simulation on two series of experiment, one was conducted on the composite slope and the other was on the flat one. The former experiment was conducted for the purpose of investigating the validity of tsunami propagation on a complex sea bottom. On the other hand, the latter experiment was conducted to check the validity of tsunami pressures acting on the cylindrical structure. This chapter shows the configurations of above to weirs of experiment.

3.1 Composite slope

The experiment of composite slope topography had been conducted by Sakakiyama et al., (2009). This experiment is referred in order to investigating the validity of tsunami propagation generated with using Eq. (1) on a complex sea bottom.

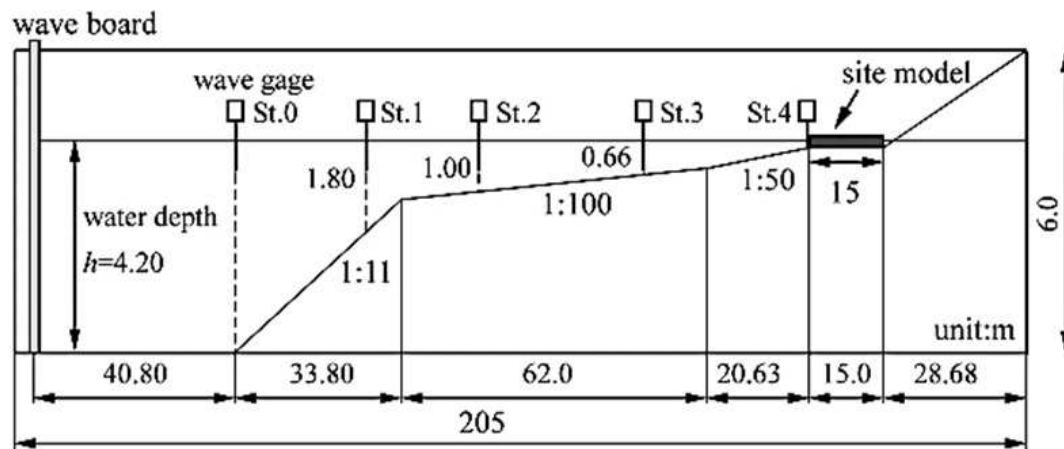


Fig. 2. Composite slope experimental setup

Two-dimensional wave flume with 205.0m in length, 6.0m in height and 3.4m in width was used in this experiment. The sea bottom consisted of several slope as shown in Fig.2. A dike with 15.0 m in length and 0.2 m in height was installed on the downstream area. The tsunami waves were generated by the wave board, which was a piston type generator, on the left hand side. In order to record the wave surface profile, wave gauges were placed at both the propagation area, i.e. $\eta_2=-89.665\text{m}$; $\eta_3=-67.225\text{m}$; $\eta_4=-33.025\text{m}$; $\eta_5=-1.5\text{m}$; $\eta_6=-0.225\text{m}$ and $\eta_7=-0.01\text{m}$ and in the inundation area, i.e. $\eta_8=+0.29\text{m}$ and $\eta_9=+0.532\text{m}$ (all locations are measured in the x-axis direction from the dike corner).

3.2 Flat bottom slop

Experiments were conducted on open channel flume with 12.0m in length, 0.4m in width and 0.4m in depth as shown in Fig. 3. Various bore heights were generated by instantaneously lifting up the division plate, which separates the downstream quiescent water from the upstream deeper water. Upstream water level (h_1) was change from 0.15m to 0.3m while the downstream water depth (h_2) was kept at 0.045m.

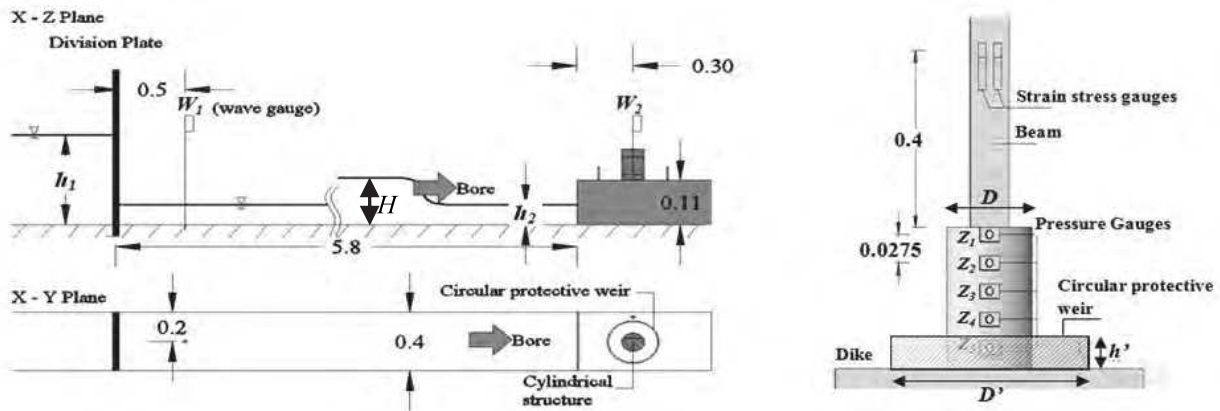


Fig. 3. Flat bottom experimental setup

At the downstream area, a dike with 0.11m height was installed 5.8m from the division plate. Cylindrical structure, which is assumed as an oil storage tank, with difference diameter (D), i.e. 0.04m, 0.08m and 0.11m, was set 0.3m from the dike’s tip.

A weir, that represents the oil protective barrier, was installed around cylindrical structure to investigate its existence effects. Building code of oil weir require certain level of weir height and weir diameter to restrain any leak from the storage material. In addition, the weir volume must be more than 1.1 times of storage volume. Regarding those conditions, this study set various diameters (D') and heights (h') as described at Table 1.

		Cylindrical structures													
		Diameter (m)													
		D=0.04			D=0.08			D=0.11							
		Wave Tank Height (m)			Wave Tank Height (m)			Wave Tank Height (m)							
Weirs		Diameter (m)	Height (m)	Type	$h_1=0.2$	$h_1=0.25$	$h_1=0.3$	$h_1=0.2$	$h_1=0.25$	$h_1=0.3$	$h_1=0.2$	$h_1=0.25$	$h_1=0.3$		
Weirs	$D'=0.26$				Diameter (m)	Height (m)	Type	$h_1=0.2$	$h_1=0.25$	$h_1=0.3$	$h_1=0.2$	$h_1=0.25$	$h_1=0.3$	$h_1=0.2$	$h_1=0.25$
		$h'=0.02$	Type A ₁	O				O	O	O	O	O	X	X	X
		$h'=0.04$	Type A ₂	O				O	O	O	O	O	O	O	O
	$D'=0.22$	Diameter (m)	Height (m)	Type	$h_1=0.2$	$h_1=0.25$	$h_1=0.3$	$h_1=0.2$	$h_1=0.25$	$h_1=0.3$	$h_1=0.2$	$h_1=0.25$	$h_1=0.3$		
					$h'=0.02$	Type B ₁	O	O	O	O	O	O	X	X	X
					$h'=0.04$	Type B ₂	O	O	O	O	O	O	O	O	O
	$D'=0.16$	Diameter (m)	Height (m)	Type	$h_1=0.2$	$h_1=0.25$	$h_1=0.3$	$h_1=0.2$	$h_1=0.25$	$h_1=0.3$	$h_1=0.2$	$h_1=0.25$	$h_1=0.3$		
					$h'=0.02$	Type C ₁	O	O	O	X	X	X	X	X	X
					$h'=0.04$	Type C ₂	O	O	O	O	O	O	X	X	X
					$h_1=0.2$	$h_1=0.25$	$h_1=0.3$	$h_1=0.2$	$h_1=0.25$	$h_1=0.3$	$h_1=0.2$	$h_1=0.25$	$h_1=0.3$		
					$h_1=0.2$	$h_1=0.25$	$h_1=0.3$	$h_1=0.2$	$h_1=0.25$	$h_1=0.3$	$h_1=0.2$	$h_1=0.25$	$h_1=0.3$		
					$h_1=0.2$	$h_1=0.25$	$h_1=0.3$	$h_1=0.2$	$h_1=0.25$	$h_1=0.3$	$h_1=0.2$	$h_1=0.25$	$h_1=0.3$		
					$h_1=0.2$	$h_1=0.25$	$h_1=0.3$	$h_1=0.2$	$h_1=0.25$	$h_1=0.3$	$h_1=0.2$	$h_1=0.25$	$h_1=0.3$		

note: O = conducted experiment

Table 1. Experiment cases

Several measurement gauges were places on specific location for verification purposes. Three wave gauges (W_1 , W_2 and W_3) and one velocity meter (V_1) were placed on the propagation area, while one wave gauges (W_4) and one velocity meter (V_2) were placed on the inundation area. As seen in Fig.5, five pressure gauges (Z_1 , Z_2 , Z_3 , Z_4 and Z_5) were attached on the front face of cylindrical structure with 0.0275m distances between two gauges to collect direct pressure data. While four strain-stress gauges were installed on the beam to obtain horizontal forces.

4. Results and discussions

4.1 Verification of simulation

4.1.1 Experimental with composite slope

Verifications are conducted on both propagation and inundation area. Fig. 4 shows the profile of water surface elevation at propagation area, i.e. η_3 , η_4 and η_5 , and at inundation area (η_8). Both experimental data and numerical simulation results are fit quite well in the bore front face and maximum wave surface elevation value. The experimental data shows the detail record of fluctuation at the tail of wave profile in η_4 and η_5 , which indicates the collision between incident wave and reflected one.

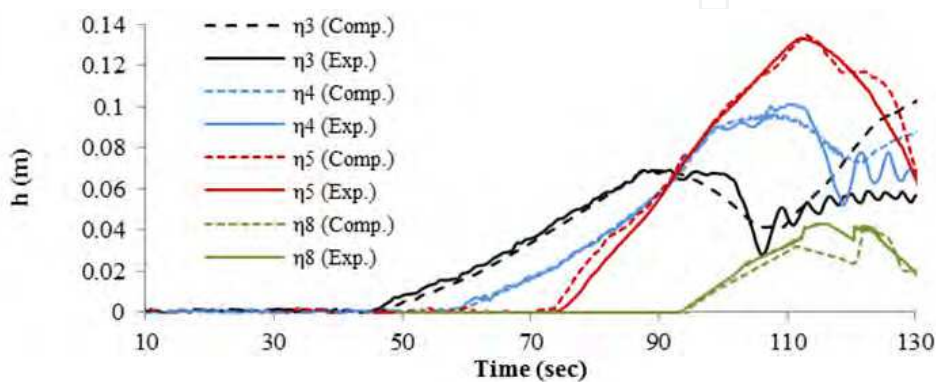


Fig. 4. Water surface elevations profiles at η_3 , η_4 , η_5 and η_8

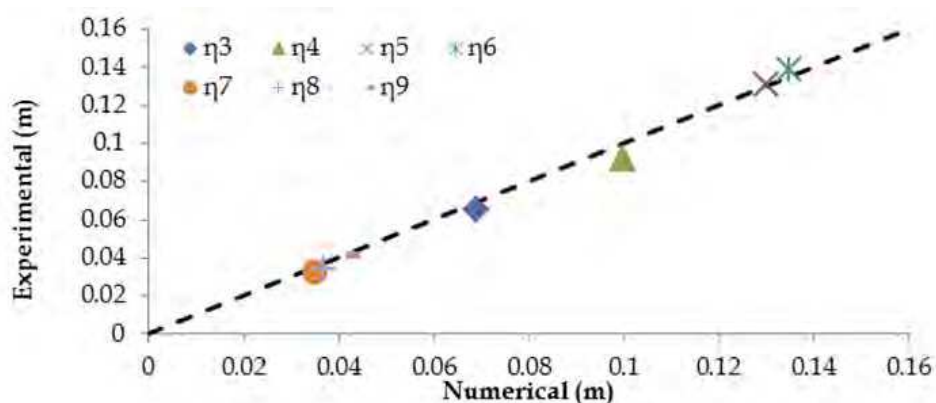


Fig. 5. Comparison of maximum water surface elevation at each measurement point

The plotted dots in the Fig. 5 are scatter close to the validity line ($h_{exp}/h_{comp} = 1$), it means that there are good agreements on the verification of maximum water surface in propagation and inundation area.

4.1.2 Experimental with bottom flat

4.1.2.1 Water surface elevation profiles

The numerical simulation of bottom flat cases also confirms the good agreement of numerical and experimental at the propagation and inundation area. Fig. 6 shows the wave profile at propagation area with the difference impoundment height, i.e. 0.15m, 0.20m and 0.25m at W_2 .

W_2 station is located 2.0m downstream side from W_1 station. In this station, water surface elevation quickly elevates when bore passes the measurement point. After sudden increase, wave constantly keeps its surface level before it fluctuates due to the collision of incident wave and reflected wave. The verifications fit well in the bore front profile, propagation phase and also the bore tail.

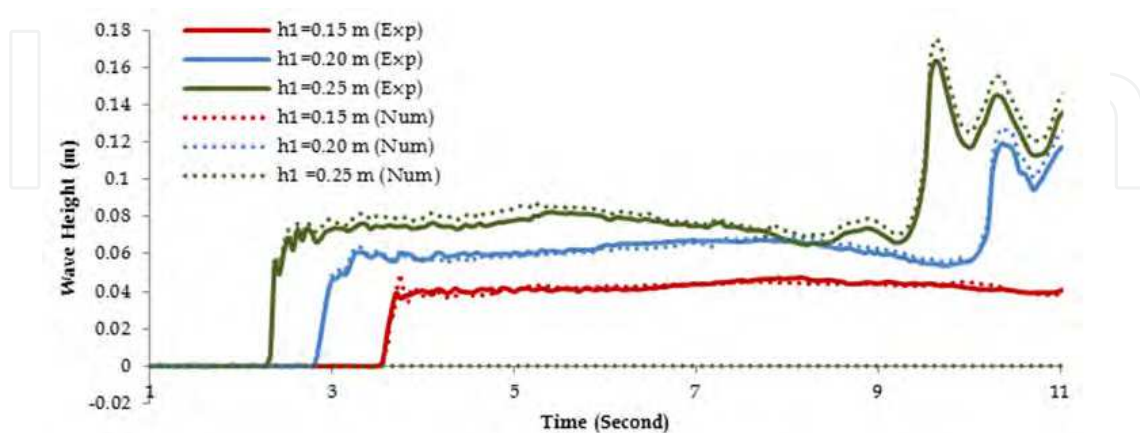


Fig. 6. Water surface elevations profiles at propagation area

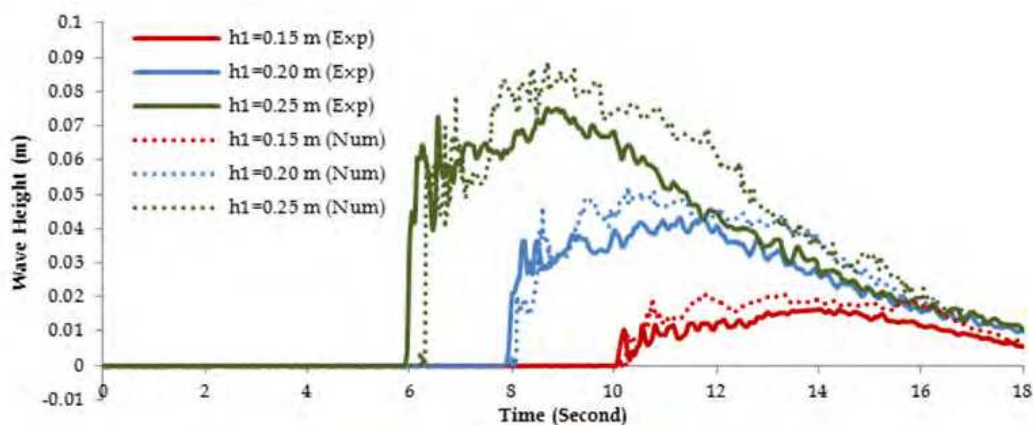


Fig. 7. Water surface elevations profiles at inundation area

Fig.7 shows the wave profile at the inundation area. Wave profile shows increasing trend after the quick raise at the beginning of measurement due to the incoming of sustain wave. Heavy fluctuations at the beginning of measurement indicate turbulence action occurs due to hydraulic wave jump hit the dike. Both experimental data and numerical result show similar trend of wave profile, though the simulations are slightly over estimate the maximum water depth after bore passes the wave gauges in the inundation area

4.1.2.2 Velocities profiles

Fig. 8 shows the verification of wave velocity with various impoundment heights in front of cylindrical structure with no weir existence. The maximum value of velocity occurs just after wave passes the current-meter. Then, the velocity profile shows the dramatic decreasing trend as the wave begins to adjust its flow after the successive waves collide with reflected ones from structure. Higher impoundment level ($h_1=0.25\text{m}$) cause high velocity value and quick wave arrival time ($t=5.9\text{s}$).

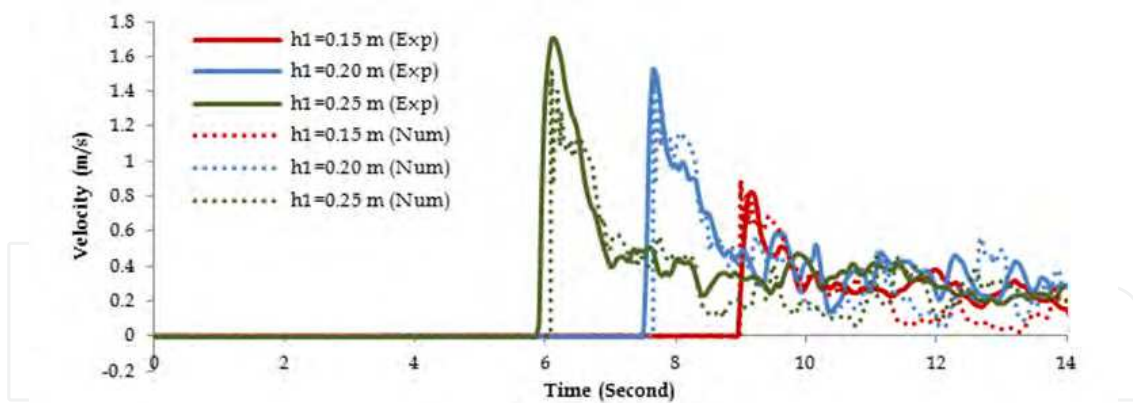


Fig. 8. Wave velocity profiles in front of cylindrical structure

Meanwhile Fig. 9 shows the wave velocity profile in the side of cylindrical structure. The quick raise velocity at the beginning of measurement also observes in this location. In addition, the slight decreasing trend indicates that the successive wave flows with less or no collision from the reflected wave.

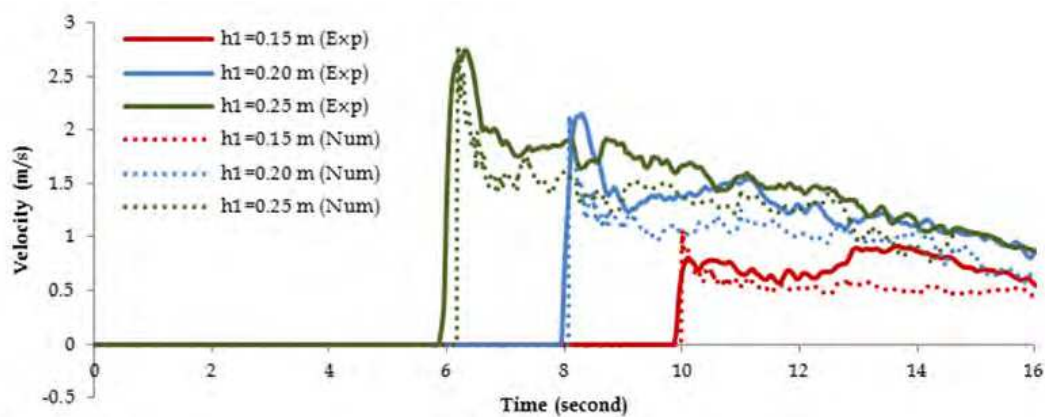


Fig. 9. Wave velocity profiles beside cylindrical structure

Fig. 8 and Fig. 9 show that even under these complicate flow conditions, the numerical results show good agreement with the experimental ones. Though at the side of structure, the numerical simulations appear to slightly overestimate the experimental results.

4.1.2.3 Force profiles

The verification of wave force acting on the 0.11m of structure diameter with various impoundment levels can be seen in Fig. 10. Both experimental and numerical results record sharp increase of initial force at the beginning of measurement as a result of wave hit the structure at the first attempt. Although the initial impact produces significant force value, it only occurs at very short period of time. Therefore there is high possibility to miss the peak of initial impact force during the observation. While sustain force, which occurs due to the accumulation of continuous incident waves, can be easily observe either in experimental or numerical results. The good agreement on these both forces can be seen in Fig. 10, while the comparison on the other maximum initial forces and maximum sustain ones can be seen in Fig. 11 (a) and 11 (b).

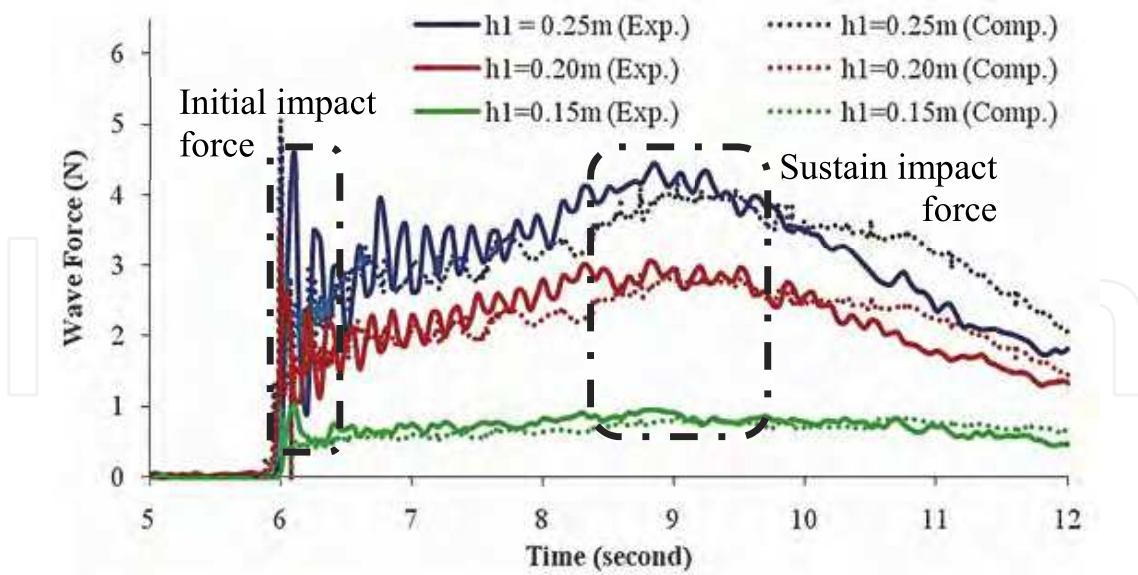


Fig. 10. Wave force profile acting on cylindrical structure.

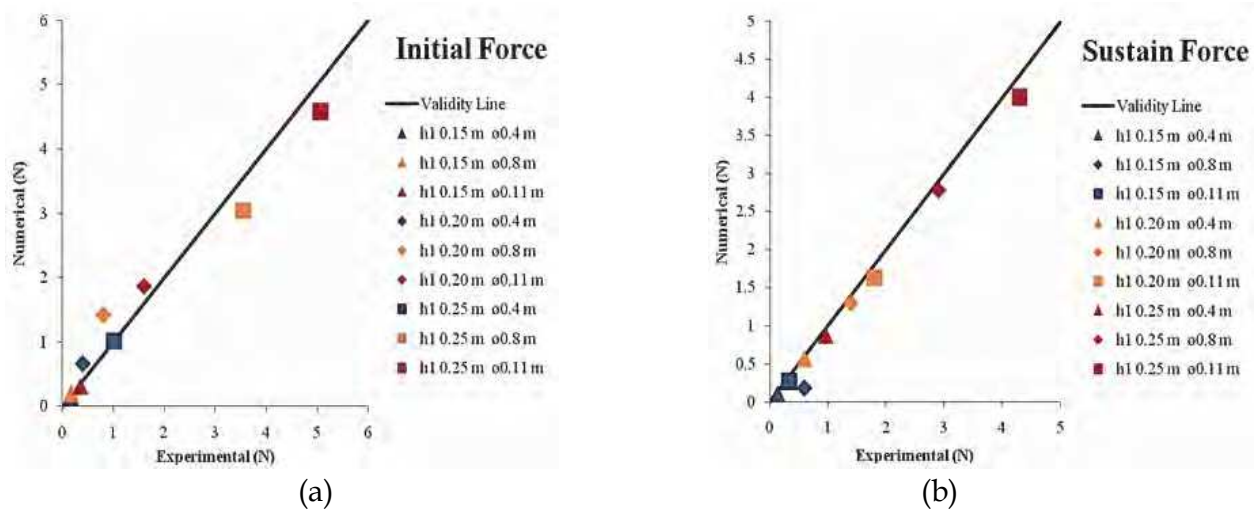


Fig. 11. Validation of maximum wave forces: (a) initial wave forces, and (b) sustain wave forces

Good agreement can be seen both in maximum initial force and maximum sustain one in the wide range of bore height. The correlation of maximum initial force is slightly lower compare to sustain one. It is due to the recording of peak values of initial impact force mainly depend on the sampling frequency of data in experimental or computational time interval in numerical simulation.

4.1.2.4 Pressure profiles

Fig. 12 shows the pressure profile of attached pressure gauge on the front face of cylindrical structure. With the 0.08m of structure diameter and 0.2m of impoundment height, this figure shows that pressure at the bottom section (Z_5) received the highest pressure, and the pressure value decrease along upper section (Z_1). Even though the initial pressure seems blurred in this case, the sustain pressure can be observed well.

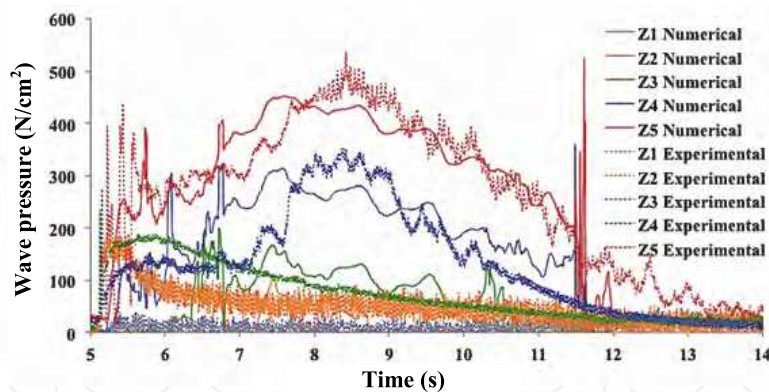


Fig. 12. Wave velocity profiles beside of cylindrical structure

The comparison between experimental and numerical results shows that numerical seems taking longer time on achieving maximum pressure ($t=8.5$ on Z_5) compare to experimental ones ($t=7.7$ on Z_5). Some spikes are also recorded on the tail of pressure profile in the computed results due to the instability of numerical simulation during complex conditions, which could be minimalized by setting up larger grid size. Overall, these comparisons show that fairly good agreement can be obtained between numerical and experimental results, both in the maximum value and the profile trend.

4.2 Cylindrical weir effects

4.2.1 Characteristic of water surface elevation

As seen in Fig. 13, the existence of cylindrical weir delays the arrival of tsunami wave inside weir area for a moment, and it decrease the initial water depth ($t=4.5s-5s$). However, after the depth of wave exceeds the weir height, the water surface level in the case with weir existence increases higher compare to without weir case. It is due to weir acts as water container and tends to kept water inside while the sustain waves are continuously flowing above it.

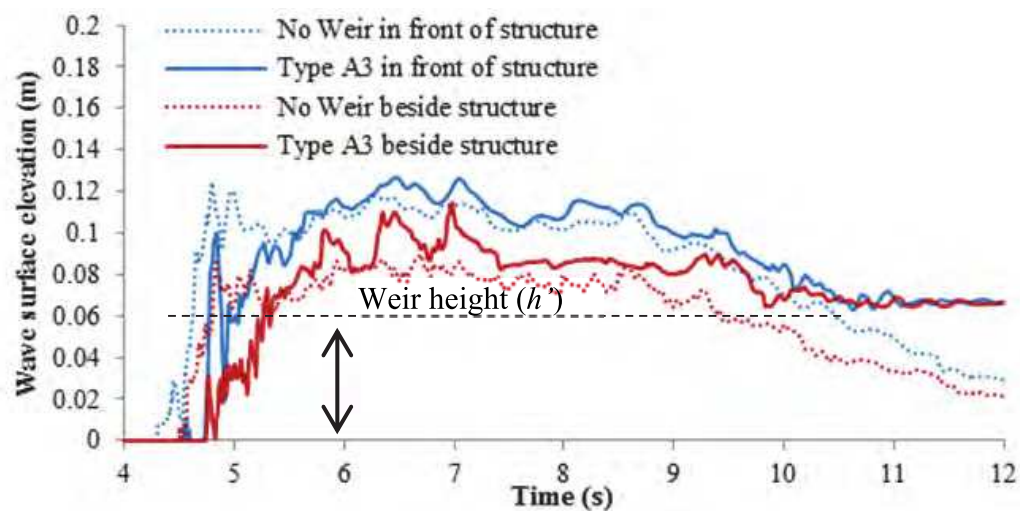


Fig. 13. Wave surface elevation profiles in front and beside cylindrical structure inside the weir area

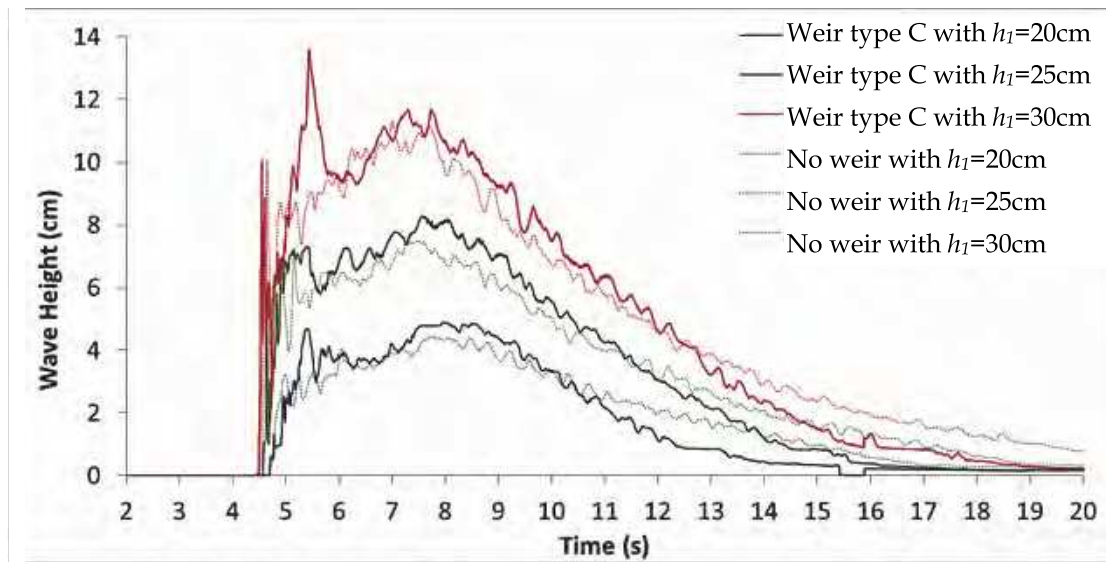


Fig. 14. Wave surface elevation profiles beside the cylindrical structure outside the weir area

The existence of weir tends to increase water surface elevation, not only inside the weir area, but also outside of it. Fig. 14 supports the evidence of increasing water depth despite of impoundment height.

4.2.2 Characteristic of velocities

The wave velocity profile just outside weir ($x=+0.16\text{m}$) and inside weir ($x=+0.19\text{m}$) in the case of no weir and weir Type A_3 can be seen in Fig. 15. This profile is recorded at $Z=+0.05\text{m}$ above the dike with $h_1=0.25\text{m}$. The weir existence cause several fluctuations in the beginning of measurement as an indication of complex motion occurs. Further, the weir existence also tends to reduce velocities at both inside and outside weir due to blocked wave passage.

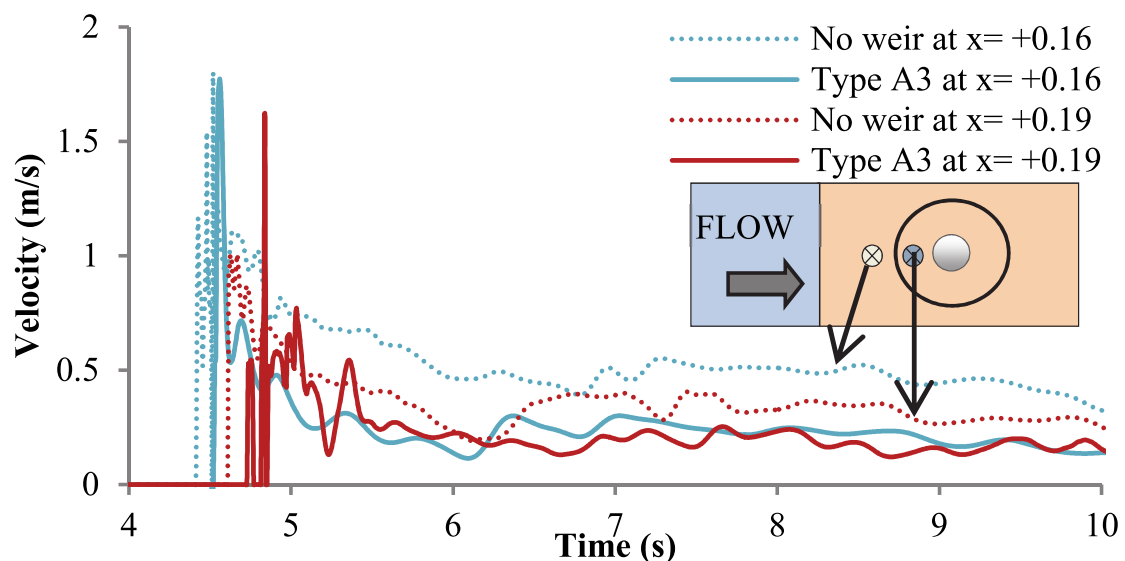


Fig. 15. Wave surface elevation profiles just in front and inside cylindrical weir

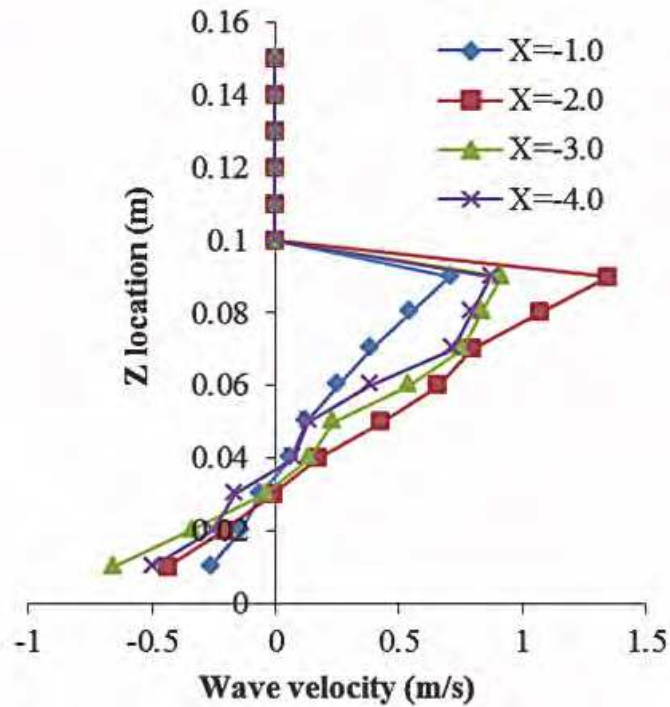


Fig. 16. Vertical distribution of wave velocity

Fig. 16 show the vertical distribution of maximum wave velocity at several location in front of structure, while Fig. 17 shows the horizontal distribution of maximum wave velocity at the bottom section, middle section and top section of structure. Fig. 16 clearly indicates the increase amount of velocity from bottom to top. The highest positive velocity occurs at $x=-0.02\text{m}$ from structure, just after the overtopped wave hit the dike. While the negative ones, which indicate the opposite direction of $x+$, occurs at the bottom section of 0.03m in front of structure.

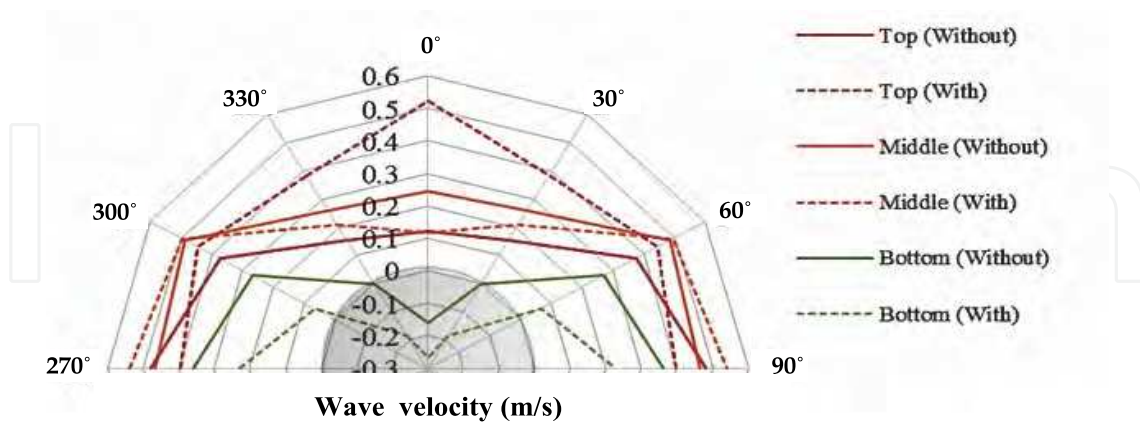


Fig. 17. Horizontal distribution of wave velocity

Fig. 17 shows that the weir existence tends to significantly increase the velocity at the top section, in front of structure. However the magnitude of increasing velocity is decreasing along circumferential direction. At the bottom section, the existence of weir causes the reduction of velocity at all circumferential faces.

4.2.3 Characteristic of pressures

The effect of the weir to the pressure mainly depends on the weir attributes, i.e. height and diameter. Fig. 18 shows the normalized pressure acting on the structure with various weir height to understand the effect of weir height in case of larger overtopped wave, i.e. $h_1=0.30\text{m}$.

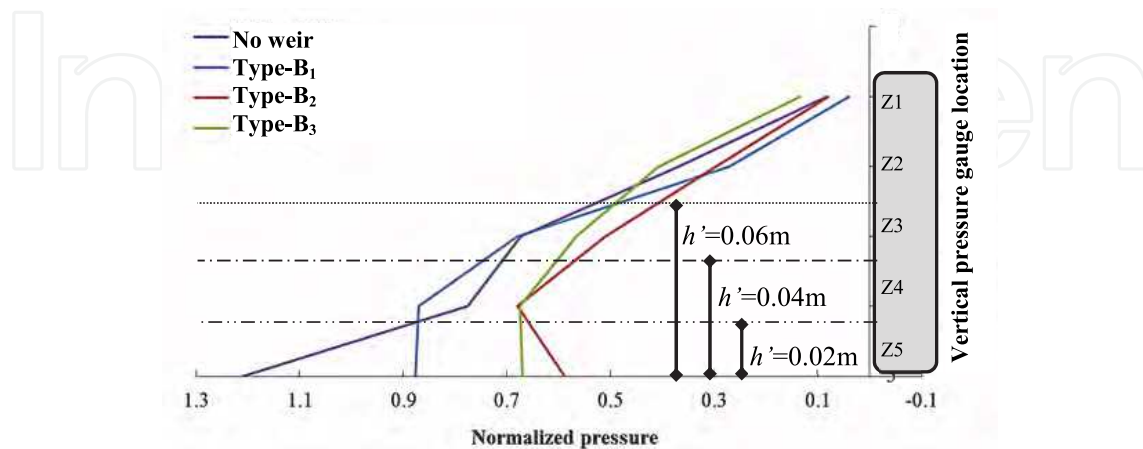


Fig. 18. Distribution of maximum sustain wave pressure on various weir height with $h_1=0.30\text{m}$



Fig. 19. Snapshots of inundation wave against weir Type B_2 with: (a) $h_1=0.03\text{m}$ caused large weir overtopping and (b) $h_1=0.02\text{m}$ caused small weir overtopping

Fig. 18 shows the vertical distribution of pressure with the normalized pressure as the horizontal axis versus location of pressure gauges as the vertical axis. Weir height successfully reduces the pressure magnitude at the bottom section in all weir height cases, especially in weir Type B_2 and B_3 . As can be seen in Fig. 19 (a), weir protects the bottom section of structure from the direct hit of initial impact. However, the reduction effect becomes less effective toward the upper section, i.e. middle and top section. The smaller differences between the case of with and without weir at the middle sections are caused by the increase water surface elevation on the front face of structure due to cylindrical weir existence. Fig 19(b) shows that $h_1=0.02\text{m}$ caused the small overtopped wave above weir. The vertical pressure distribution characteristic acting on the structure at this condition is similar with the larger overtopped cases.

Meanwhile, the effect of weir diameter can be described base on the amount of overtopped wave above protective weir. The vertical distribution of wave pressure in case of large overtopped wave is shown in Fig. 20 (a), while in case of small overtopped ones is shown in Fig. 20 (b). Both figures use cylindrical structure with 0.04m of diameter with various weir diameters, i.e. 0.26m, 0.22m and 0.16m. It means that the space size between inner face of cylindrical weir and outer face of cylindrical structure are 0.11m, 0.10m and 0.06m for Type A_1 , type B_1 and type C_1 respectively.

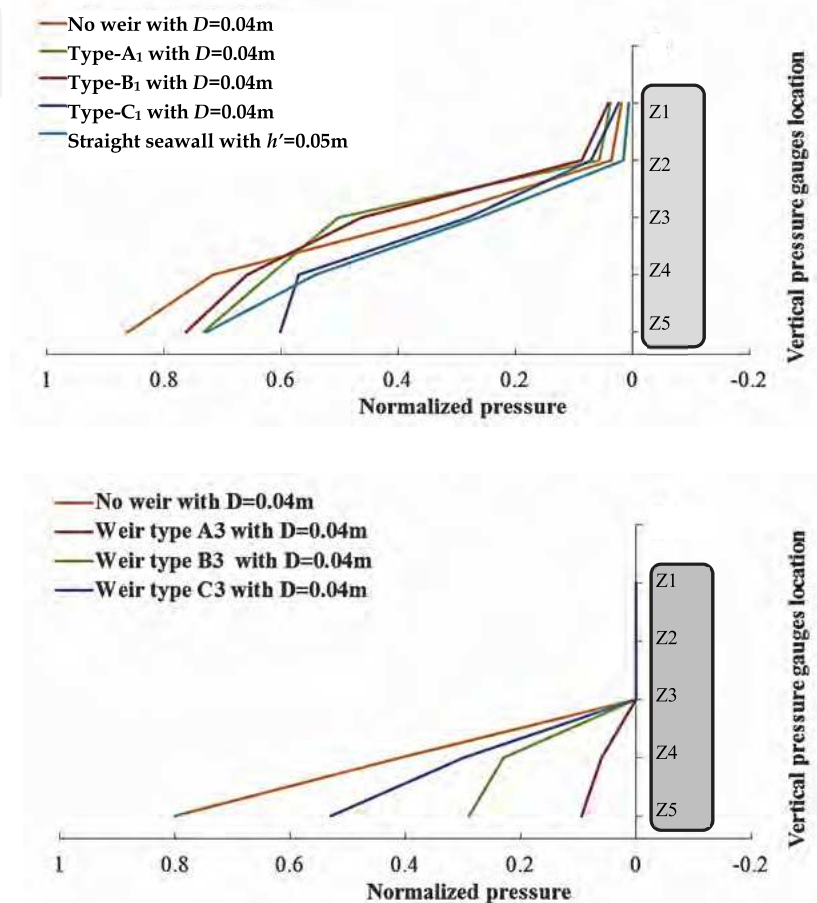


Fig. 20. Distribution of maximum sustain wave pressure on various weir diameter with: (a) larger overtopped wave $h_1=0.25m$, and (b) small overtopped wave $h_1=0.20m$

In case of larger wave overtopped, smaller space size, i.e. weir Type C_1 , tended to the effectively reduce the wave pressure. The limited space between weir and structure cause wave difficult to accelerate their motion. In Fig. 20 (a), the establishment of straight seawall with height 0.05m at the dike corner (Wijatmiko and Keisuke, 2010b) have similar effect to the existence of smaller weir diameter. Seawall height cause shallower inundation depth due to small-overtopped wave and seawall location give adequate space for the wave to adjust their motion after hitting the dike.

Meanwhile in the smaller wave overtopped cases, the wider weir causes the pressure against structure significantly reduce. It is because with the similar volume of overtopped water flow, the wider diameter caused the inundation depth become shallower in the comparison with smaller weir diameter.

The horizontal distribution of maximum sustain wave pressure at the several vertical locations can be seen in Fig. 21(a), 21(b) and 21(c). The maximum water surface elevation around the cylindrical structure was 0.12m, therefore $z=+0.01\text{m}$ represents bottom section, $z=+0.05\text{m}$ is the middle section and $z=+0.09\text{m}$ is the top section. 0 degree in the chart axis indicates the front face of structure, which is parallel to the direction of incoming wave, while the 90 degree and 270 degree indicate side face of the cylindrical structure.

As seen in Fig. 21, pressures at the front side of cylindrical structure are reduced due to the existence of weir in this section. However, this reduction effect becomes smaller along circumferential direction. While at the middle and top section, the existence of weir tend to increase the pressure magnitude due to the increase of water depth around cylindrical structure.

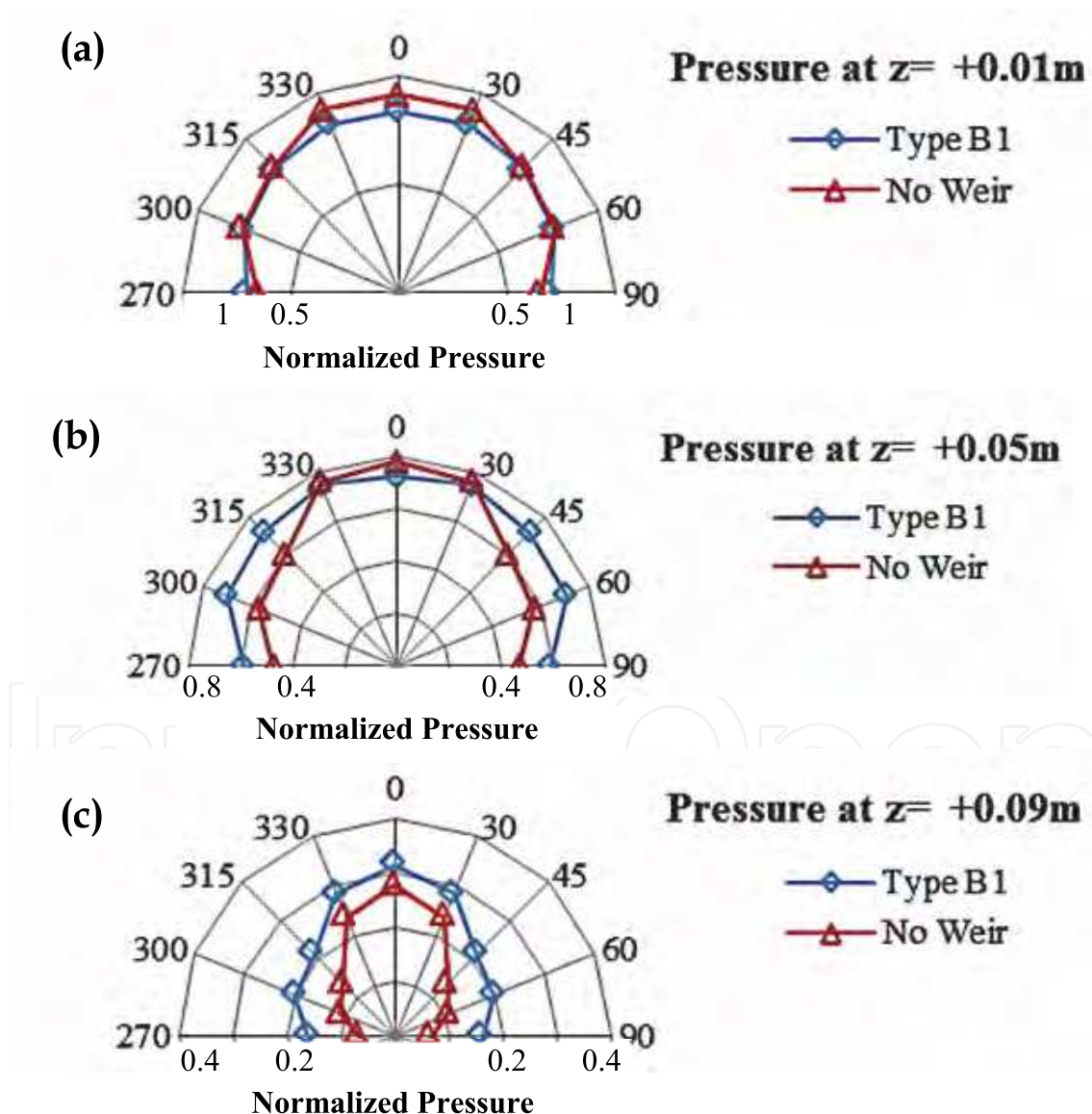


Fig. 21. Horizontal wave pressure distribution on without weir and weir type B_1 case: (a) at top section, (b) at middle section and (c) at bottom section.

4.2.4 Characteristic of forces

Weir existence reduces wave force in all impoundment height and all weir diameters cases. In addition, the reduction effect varies depending on the space between weir and structure. Higher force at Type B_1 in the cases of larger overtopped wave ($h_1=0.25\text{m}$ and $h_1=0.30\text{m}$) are caused by direct hit by overtopped flow to the cylindrical structure, while the limited space between weir and structure cause significant reduction of wave forces at Type C_1 , as seen in Fig. 22.

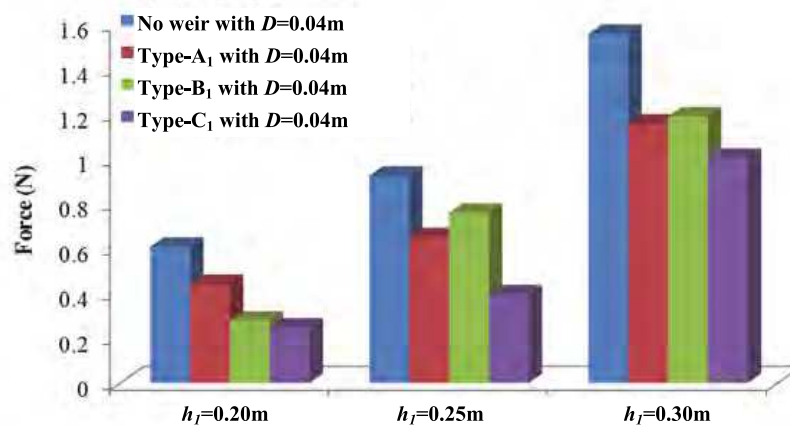


Fig. 22. Maximum sustain wave force

Meanwhile in the smaller overtopped wave case ($h_1=0.02\text{m}$), the shallower inundation depth inside weir cause the significant reduction of wave force. In these cases, the larger weir diameter, which means the closer weir to the dike corner, cause amount of overtopped wave inside the weir becomes larger compare to smaller ones.

5. Conclusions

The interactions between a single bore and cylindrical structure with cylindrical weir, supposed as oil tank barrier, are investigated through experimental and numerical study. Analytical equation to obtain the input velocities profile from the water surface elevation is introduced as well. Good agreements are confirmed in the physical principal quantities between experimental and numerical simulation both in the simple flat bottom and complex slope bottom conditions.

The existence of cylindrical weir tends to delay the arrival time of wave inside the weir area, and increases the water surface level around structure. In addition, weir tends to effectively reduce velocity at the bottom section, but in the contrary there are increasing velocities at upper section due to series of successive wave flowing above cylindrical weir. The reduction effects on velocity at the bottom section may provide some advantages for mitigating the scouring problems.

At the vertical pressure distributions, cylindrical weir also effectively reduces wave pressure at the bottom section. However, the reduction effect becomes smaller along higher section. While at the horizontal pressure distribution, the cylindrical weir tends to reduce pressure at the front face of structure. Furthermore, the weir configuration, i.e. weir height and weir diameter, and the level of overtopped wave play important role on the pressure and force magnitude.

6. Acknowledgment

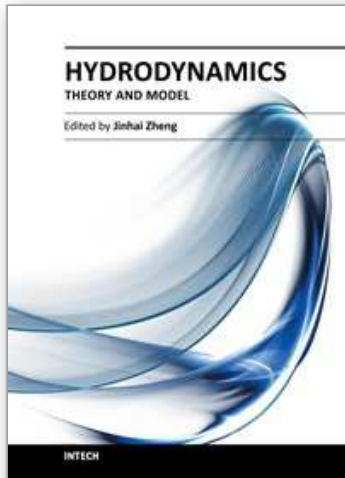
This study was carried out by the financial support of Ministry of Education, Culture, Sport, Science, and Technology of Japan through Monbuka-gakusho scholarship. The authors would like to thank you Dr. Sakakiyama, T. for allowing us to use their experimental data. The numerical source codes used in this study are developed by research group, which are organized by Coastal Development Institute of Technology (CDIT). Some materials in this chapter are summarized from Wijatmiko and Murakami, 2010a, 2010b, 2011. All contributions are acknowledged.

7. References

- Arikawa, T., and T. Yamano (2008). Large Scale Simulation on Impulsive Wave Pressure by using CADMAS SURF/3D, *Annual Journal of Civil Engineering in the Ocean (JSCE)*, Vol. 55, pp.26-30 (in Japanese)
- Dangerous Goods Safety Management (2003). Spills Containment and Clean-up Measures for Dangerous Goods and Combustible Liquids. *Dangerous Goods Safety Management Act 2001*, Queensland Government Counter Disaster and Rescue Services.
- Federal Emergency Management Agency (2008). Guidelines for Design of Structures for Vertical Evacuation from Tsunamis, FEMA, Retrieved from <http://www.fema.gov/library/viewRecord.do?id=3463>
- Fukui, Y., S. Hidehiko, M. Nakamura, and Y. Sasaki (1962a). Study on Tsunami, *Annual Journal of Coastal Engineering in Japan*, Vol. 9, pp. 44-49 (in Japanese).
- Goto, H., H. Ikari, K. Tonono, T. Shibata, T. Harada, and A. Mizoe (2009). Numerical Analysis on Drifting Behavior of Container on Apron due to Tsunami by Particle Method, *Annual Journal of Civil Engineering in the Ocean (JSCE)*, Vol. 59, pp.261-265 (in Japanese)
- Haritos, N., Ngo, T., and Mendis, P. (2005). Evaluating Tsunami Wave Force on Structures, *Proceedings of International Symposium Disaster Reduction on Coasts Scientific-Sustainable-Holistic-Accessible*. Monash University, Melbourne, Australia, 2005
- Hirt, C.W., and Nichols, B.D. (1981). Volume of fluid (VOF) method for dynamics of free boundaries. *Journal of Computational Physics*. Vol. 39, pp.201-225.
- International Energy Agency (15 March 2011). Impact of Earthquakes and Tsunamis on Energy Sectors in Japan, In : *International Energy Agency Reports*, 20 May 2011, Available from : <http://www.iea.org/files/japanfactsheet.pdf>
- Kawasaki, K., S. Yamaguchi, N. Hakamada, N. Mizutani, and S. Miyajima (2006). Wave Pressure Acting on Drifting Body after Collision with Bore, *Annual Journal of Civil Engineering in the Ocean (JSCE)*, Vol. 53, pp. 786-790
- Lukkunaprasit, P., Ruangrassamee, A., and Thanasisathit, N. (2009). Tsunami loading on buildings with openings, *Science of Tsunami Hazard*, Vol. 28, No. 5, pp. 303-310
- Mizutani, S., and F. Imamura (2001). Dynamic wave force tsunami acting on structure, *Proceeding of International Tsunami Symposium*, pp. 941-948
- Okada, T., T. Sugano, T. Ishikawa, T. Ohgi, S. Takai, and C. Hamabe (2004). Structural Design Method of Building for Tsunami Resistance (proposed), *Building Technology Research Institute*, The Building Center of Japan.

- Palermo, D., and Nistor, I. (2008). Understanding tsunami risk to structures : a Canadian perspective, *Science of Tsunami Hazards*, Vol. 27, No. 4, pp.1-11.
- Sakakiyama, T., and R. Kajima (1992). Numerical simulation of nonlinear waves interacting with permeable breakwaters. *Proceedings of the 23rd International Conference on Coastal Engineer*, ASCE, pp. 1517-1530
- Sakakiyama, T., S. Matura, and M. Matsuyama (2009). Tsunami Force Acting on Oil Tanks and Buckling Analysis for Tsunami Pressure, *Journal of Disaster Research*, Vol. 4, No. 6, pp. 427-434
- Tomita, T., K. Honda, and T. Kakinuma (2006). Application of three-dimensional tsunami to estimation of tsunami behavior around structures, *International Conference on Coastal Engineering*, pp. 1677-1688
- Wijatmiko, I., and Murakami, K. (2010a). Numerical Simulation of Tsunami Bore Pressure on Cylindrical Structure, *Annual Journal of Civil Engineering in the Ocean (JSCE)*, Vol. 26, pp. 273-278, ISSN 0912-7348
- Wijatmiko, I., and Murakami, K. (2010b). Three Dimensional Numerical Simulation of Bore Type Tsunami Propagation and Run up on to a Dike, *Journal of Hydrodynamics, Ser. B*, Vol. 22, Issue 5, Supplement 1, pp.259-264, ISSN 1001-6058
- Wijatmiko, I., and Murakami, K. (2010a). Tsunami Bore Pressures and Forces Acting On the Structures Surrounded by weir, *Annual Journal of Civil Engineering in the Ocean (JSCE)*, Vol. 27, pp. 286-290, ISSN 0912-7348
- Yeh, H. (2007). Design Tsunami Forces for Onshore Structures, *Journal of Disaster Research*, Vol 2, No. 6, pp. 531-536
- Yeh, H. (1991). Tsunami Bore Runup, *Natural Hazard*, Vol. 4, pp.209-220.
- Youngs, D.L. (1982). Time-dependent multi material flow with large fluid distraction. In : *Numerical Methods for Fluid Dynamics*, Morton, K., and Baines, M. (Eds.),pp.273-285, Academic Press, New York.

IntechOpen



Hydrodynamics - Theory and Model

Edited by Dr. Jin - Hai Zheng

ISBN 978-953-51-0130-7

Hard cover, 306 pages

Publisher InTech

Published online 14, March, 2012

Published in print edition March, 2012

With the amazing advances of scientific research, Hydrodynamics - Theory and Application presents the engineering applications of hydrodynamics from many countries around the world. A wide range of topics are covered in this book, including the theoretical, experimental, and numerical investigations on various subjects related to hydrodynamic problems. The book consists of twelve chapters, each of which is edited separately and deals with a specific topic. The book is intended to be a useful reference to the readers who are working in this field.

How to reference

In order to correctly reference this scholarly work, feel free to copy and paste the following:

I. Wijatmiko and K. Murakami (2012). Study on the Interaction Between Tsunami Bore and Cylindrical Structure with Weir, Hydrodynamics - Theory and Model, Dr. Jin - Hai Zheng (Ed.), ISBN: 978-953-51-0130-7, InTech, Available from: <http://www.intechopen.com/books/hydrodynamics-theory-and-model/study-on-the-interaction-between-tsunami-bore-and-cylindrical-structure-with-weir>

INTECH
open science | open minds

InTech Europe

University Campus STeP Ri
Slavka Krautzeka 83/A
51000 Rijeka, Croatia
Phone: +385 (51) 770 447
Fax: +385 (51) 686 166
www.intechopen.com

InTech China

Unit 405, Office Block, Hotel Equatorial Shanghai
No.65, Yan An Road (West), Shanghai, 200040, China
中国上海市延安西路65号上海国际贵都大饭店办公楼405单元
Phone: +86-21-62489820
Fax: +86-21-62489821

© 2012 The Author(s). Licensee IntechOpen. This is an open access article distributed under the terms of the [Creative Commons Attribution 3.0 License](#), which permits unrestricted use, distribution, and reproduction in any medium, provided the original work is properly cited.

IntechOpen

IntechOpen